Asymmetric Lumino-Transformer: Circularly Polarized Luminescence of Chiral Eu(III) Coordination Polymer with Phase-Transition Behavior

Makoto Tsurui,[1] Yuichi Kitagawa,[2,3] Sunao Shoji,[2,3] Hitomi Ohmagari,[4] Miki Hasegawa,[4] Masayuki Gon,[5] Kazuo Tanaka,[5] Masato Kobayashi,[3,6] Tetsuya Taketsugu,[3,6] Koji Fushimi,[2] and Yasuchika Hasegawa[*2,3]*

[1]Graduate School of Chemical Sciences and Engineering, Hokkaido University, Kita 13, Nishi 8, Kita-ku, Sapporo, Hokkaido 060-8628, Japan.

[2]Faculty of Engineering, Hokkaido University, Kita 13, Nishi 8, Kita-ku Sapporo, 060-8628, Japan.

[3]Institute for Chemical Reaction Design and Discovery (WPI-ICReDD), Hokkaido University, Kita 21, Nishi 10, Kita-ku, Sapporo, Hokkaido 001-0021, Japan.

[4]College of Science and Engineering, Aoyama Gakuin University, 5-10-1 Fuchinobe, Chuo-ku, Sagamihara, Kanagawa 252-5258, Japan.

[5]Graduate School of Engineering, Kyoto University, Kyoto daigaku-katsura, Nishikyo-ku, Kyoto 615-8510, Japan.

[6]Faculty of Science, Hokkaido University, Kita 10, Nishi 8, Kita-ku, Sapporo, Hokkaido 060-0810, Japan.

Abstract

A chiral Eu(III) coordination polymer with phase-transition behavior, $[Eu(+tfc)_3(m\text{-dpeb})]_n$, (+tfc: (+)-3-trifluoroacetylcamphorato, *m*-dpeb: 1,3-bis(diphenylphosphorylethynyl)benzene) was reported for understanding the effect of polymer chain arrangement (orientation effect) on the circularly polarized luminescence (CPL) in a solid system. The phase-transition behavior of the transformable Eu(III) coordination polymer was characterized using differential scanning calorimetry and powder X-ray diffraction. The Eu(III) coordination polymer exhibited a phase-transition at approximately 180 °C. The magnitude of the CPL intensity was drastically changed because of the phase-transition, without coordination geometrical change around the Eu(III) ion. In this study, the orientation effect of a chiral Eu(III) coordination polymer on the CPL properties in crystalline solid is demonstrated.

Introduction

Chiral luminophores, such as organic molecules, transition metal complexes, and lanthanide complexes, exhibit circularly polarized luminescence (CPL).[1–3] Recently, CPL has attracted attention for the development of security tags, three-dimensional displays, and bio-imaging applications.[4–12] The magnitude of the dissymmetry factor of CPL (g_{CPL}) is defined by the following equation:[2,11]

$$g_{CPL} = \frac{2(I_L - I_R)}{I_L + I_R}, \quad (1)$$

where I_L and I_R are the intensities of the left- and right-handed circularly polarized light, respectively. The g_{CPL} value depends on the electronic transitions of the luminescent molecule. In particular, chiral Eu(III) complexes exhibit relatively large g_{CPL} values ($g_{CPL} > 10^{-1}$) compared with chiral organic molecules and transition metal complexes ($g_{CPL} = 10^{-1} \sim 10^{-4}$).[6,9–15] Their characteristically large g_{CPL} values are based on the combination of the magnetic dipole transition in 4f orbitals and the formation of chiral steric and electronic structures induced by the organic ligands.

A series of Eu(III) complexes with chiral organic ligands, such as camphor, Pybox, naphthol, and helicene derivatives have been reported.[4,16–24] The CPL properties of chiral Eu(III) complexes are closely related to their coordination geometries and structural strain of ligands. Yuasa demonstrated that the *cis*-*trans* isomerization of the bidentate phosphine oxide ligand in a chiral Eu(III) complex leads to CPL sign inversion.[25] We also reported that a large structural strain of the β-diketonate ligands in chiral Eu(III) complexes promotes the enhancement of the ligand-to-metal charge transfer (LMCT) transition probability and increases the g_{CPL} value.[26] These results were mainly caused by the modification of the steric structure around Eu(III) ions.

The helical aggregation of chiral Eu(III) compounds in a solution also influences the magnitude of the g_{CPL} value.[27] To elucidate the relationship between the molecular orientation and the CPL properties, we focus on the chiral Eu(III) compound with structural transformation in the solid state.

Herein, chiral Eu(III) coordination polymers with phase-transition behaviors are reported for the evaluation of molecular orientations in crystalline solids. In molecular designs for the thermal phase-transition, a flexible transformation ability and a thermostable rigid structure of Eu(III) coordination compounds are required. Eu(III) coordination polymers exhibit tight stacking structures of one-dimensional polymer chains in the crystal, resulting in the formation of thermostable properties (decomposition temperature > 300 °C).[28–30] We also found that the ethynyl groups of the linker ligands in Eu(III) coordination polymers exhibit phase-transition behavior in the solid state.[31,32]

In this study, chiral Eu(III) coordination polymers with ethynyl groups in the linker ligands, $[Eu(+tfc)_3(m\text{-dpeb})]_n$ and $[Eu(+tfc)_3(p\text{-dpeb})]_n$, were prepared by the reaction of $[Eu(+tfc)_3(H_2O)_2]$ with *m*- or *p*-dpeb (Figure 1a, +tfc: (+)-3-trifluoroacetylcamphorato, *m*-dpeb: 1,3-bis(diphenylphosphorylethynyl)benzene, *p*-dpeb: 1,4-bis(diphenylphosphorylethynyl)benzene). The coordination polymers are composed of Eu(III) ions, chiral camphorate ligands (+tfc), and *m*- or *p*-linked phosphine oxide ligands, including ethynyl groups (*m*-dpeb or *p*-dpeb). The *o*-linked ethynyl ligand (*o*-dpeb: 1,2-bis(diphenylphosphorylethynyl)benzene) provides a mononuclear Eu(III) complex $[Eu(+tfc)_3(o\text{-dpeb})]$ (SI: Figure S7). The phase-transition behavior of Eu(III) coordination polymers was characterized using thermogravimetry (TG), differential scanning calorimetry (DSC), and powder X-ray diffraction (PXRD). The chiral Eu(III) coordination polymer, $[Eu(+tfc)_3(m\text{-}$

dpeb)]$_n$, exhibit phase-transition behavior without changes in the coordination geometry (see Figure 1b for images of Type-A and Type-B), although [Eu(+tfc)$_3$(*p*-dpeb)]$_n$ has no phase-transition temperature. The phase-transition of [Eu(+tfc)$_3$(*m*-dpeb)]$_n$ leads to a considerable change in the CPL signal intensity without a spectral shape change in the emission. Transformable chiral Eu(III) coordination polymer has been demonstrated for understanding the orientation effect on CPL properties in solid systems.

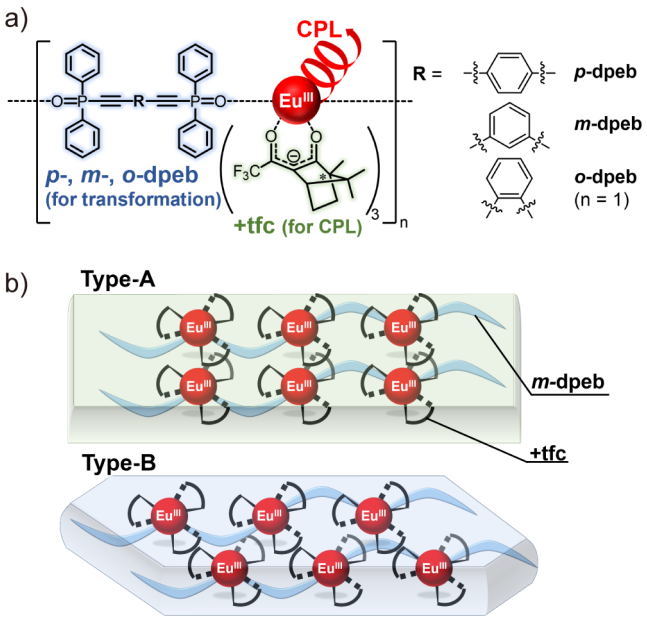

Figure 1. a) Chemical structures of [Eu(+tfc)$_3$(*p*-dpeb)]$_n$, [Eu(+tfc)$_3$(*m*-dpeb)]$_n$, and [Eu(+tfc)$_3$(*o*-dpeb)]. b) Schematic image of phase-transition in [Eu(+tfc)$_3$(*m*-dpeb)]$_n$.

Experimental Section

General methods: All chemicals were reagent grade and used without further purification. Fourier Transform infrared (FT-IR) spectra were recorded on a JASCO FT/IR-4600 spectrometer. ESI-MS spectra were measured using a JEOL JMS-T100LP. Elemental analyses were performed on an Exeter Analytical CE440. ^{1}H NMR (400 MHz) and ^{31}P NMR (162 MHz) spectra were recorded on a JEOL ECS400 at 298 K. Tetramethylsilane (δ_H = 0.00 ppm) and phosphoric acid (δ_P = 0.00 ppm) were used as internal references for ^{1}H and ^{31}P NMR, respectively. DSC was performed on a Hitachi High-Tech DSC 7020 under nitrogen atmosphere at a heating rate of 5 °C min^{-1}. TG analysis was performed on a Hitachi High-Tech TG/DTA6300 analyzer under nitrogen atmosphere at a heating rate of 5 °C min^{-1}. Synchrotron X-ray powder diffraction data were acquired using a large Debye–Scherrer camera installed at the SPring-8 BL02B2 beamline, employing an auto sampler with a multiple MYTHEN detector.[33] The wavelength of the incident X-ray was 0.800168 Å, which was calibrated using a cerium oxide standard powder sample by the National Institute of Standards and Technology. Temperature-dependent X-ray diffractometry was performed on a Rigaku SmartLab using Cu-Kα radiation (λ = 1.5418 Å).

Preparation of 1,3-bis(diphenylphosphorylethynyl)benzene (*m*-dpeb): *m*-dpeb was prepared with the procedure described in a previous report.[31] The 1,3-diethynylbenzene (1.0 g, 7.9 mmol) was dissolved in dry diethyl ether (50 mL), and the mixture was degassed by Ar bubbling. A solution of *n*-BuLi (ca. 1.6 mol L^{-1}, 12 mL, 19 mmol) was added dropwise to the solution at −80 °C. The mixture was allowed to stir for 3.5 h at −10 °C, after which chlorodiphenylphosphine (3.5 mL, 19 mmol) was added dropwise at −80 °C. The mixture was gradually brought to room temperature and stirred for 19 h. The reaction mixture was poured into

distilled water and extracted with dichloromethane. The extracts were washed with brine three times and dried over anhydrous $MgSO_4$. The solvent was evaporated, and the obtained yellow oil was placed with dichloromethane (10 mL) in a flask. The solution was cooled to 0 °C, and then an aqueous 30% hydrogen peroxide solution (10 mL) was added dropwise to the above solution. The solution was stirred for 3 h. After separation of aqueous hydrogen peroxide solution, the solution was washed with distilled water. Anhydrous $MgSO_4$ was added to the organic phases for dehydration. After filtration, the organic phase was evaporated to give a white powder. The powder was recrystallized from methanol solution to give prism crystals. Yield: 3.48 g (6.6 mmol, 84%). ^{1}H NMR ($CDCl_3$): δ = 7.92-7.86 (m, 8H), 7.83 (s, 1H), 7.68 (d, *J* = 1.8 Hz, 1H), 7.66 (d, *J* = 1.3 Hz, 1H), 7.61-7.49 (m, 12H), 7.42 ppm (t, *J* = 7.9 Hz, 1H). ^{31}P NMR (160 MHz, $CDCl_3$, 25 °C): δ = 8.26 ppm. IR (ATR): ν = 3020-3050 (st, ArC-H), 2168 (st, C≡C), 1205 cm^{-1} (st, P=O). ESI-MS (*m*/*z*): $[M+H]^+$ calcd. for $C_{34}H_{25}O_2P_2$, 527.13; found, 527.13. Anal. calcd. for $C_{34}H_{24}O_2P_2$, C 77.56, H 4.59; found, C 77.41, H 4.49%.

Preparation of $[Eu(+tfc)_3(m\text{-dpeb})]_n$ (+tfc: (+)-3-trifluoroacetylcamphorato): Europium(III) acetate *n*-hydrate (0.36 g) was dissolved in distilled water (150 mL), and a few drops of 28% ammonia solution were added. (+)-3-triflouroacetylcamphor (0.50 g, 2.0 mmol) in methanol (15 mL) was added to the solution, and the mixture was stirred for 4 h at room temperature. The reaction mixture was evaporated. The obtained powder was washed with distilled water, and the powder was dried in vacuo ($[Eu(+tfc)_3(H_2O)_2]$, 0.41 g). $[Eu(+tfc)_3(H_2O)_2]$ (0.37 g, 0.40 mmol) and *m*-dpeb (0.19 g, 0.36 mmol) were dissolved in methanol (10 mL) and refluxed for 5 h. The reaction solution was cooled to room temperature and evaporated to give a light yellow powder. The obtained powder was washed with diethyl ether and hexane. The powder was dried in vacuo

and heated at 140 ℃ for 30 min to crystallize. Yield: 0.09 g (0.06 mmol, 18% for monomer). IR (ATR): ν = 2870-2990 (st, ArC-H), 2172 (st, C≡C), 1654 (st, C=O), 1197 cm^{-1} (st, P=O). ESI-MS (*m*/*z*): $[M-tfc]^+$ calcd. for $C_{58}H_{52}EuF_6O_6P_2$, 1173.24; found, 1173.24. Anal. calcd. for $C_{70}H_{66}EuF_9O_8P_2$, C 59.20, H 4.68; found, C 58.61, H 4.66%.

Preparation of 1,4-bis(diphenylphosphorylethynyl)benzene (*p*-dpeb): *p*-dpeb was synthesized by the similar procedure as described for the *m*-dpeb, starting from 1,4-diethynylbenzene (0.63 g, 6.6 mmol), and recrystallized from methanol and dichloromethane solution, yielding prism crystals. Yield: 1.97 g (3.7 mmol, 75%). ^1H NMR ($CDCl_3$): δ = 7.85-7.92 (m, 8H), 7.60 (s, 4H), 7.55-7.59 (m, 4H), 7.48-7.54 ppm (m, 8H). ^{31}P NMR ($CDCl_3$): δ = 8.37 ppm. IR (ATR): ν = 3030-3076 (st, ArC-H), 2180 (st, C≡C), 1196 cm^{-1} (st, P=O). ESI-MS (*m*/*z*): $[M+H]^+$ calcd. for $C_{34}H_{25}O_2P_2$, 527.13; found, 527.13. Anal. calcd. for $C_{34}H_{24}O_2P_2$, C 77.56, H 4.59; found, C 77.44, H 4.49%.

Preparation of $[Eu(+tfc)_3(p\text{-dpeb})]_n$: $[Eu(+tfc)_3(p\text{-dpeb})]_n$ was synthesized by the similar procedure as described for the $[Eu(+tfc)_3(m\text{-dpeb})]_n$, starting from *p*-dpeb (0.18 g, 0.33 mmol), yielding a white powder.

Yield: 0.17 g (0.12 mmol, 35%; for monomer). IR (ATR): 2865-2990 (st, ArC-H), 2183 (st, C≡C), 1660 (st, C=O), 1179 cm^{-1}(st, P=O). ESI-MS (*m*/*z*): $[M-tfc]^+$ calcd. for $C_{58}H_{52}EuF_6O_6P_2$, 1173.24; found, 1173.25. Anal. calcd. for $C_{70}H_{66}EuF_9O_8P_2$, C 59.20, H 4.68; found, C 58.87, H 4.57%.

Optical Measurements: Emission and excitation spectra were recorded on a HORIBA Fluorolog-3 spectrofluorometer and corrected for the response of the detector system. Emission decay profiles were measured using the third harmonics (355 nm) of a Q-switched Nd:YAG laser (Spectra Physics, INDI-50, FWHM = 5 ns, λ = 1064 nm) and a photomultiplier (Hamamatsu Photonics, R5108, response time $\leq$ 1.1 ns). The Nd:YAG laser response was monitored with a digital oscilloscope (Sony Tektronix, TDS3052, 500 MHz) synchronized to the single-pulse excitation. Emission lifetimes were determined from the slope of logarithmic plots of the decay profiles. Emission lifetimes in the range of 100 to 350 K were measured by using a cryostat (Thermal Block Company, SA-SB245T) and a temperature controller (Oxford, Instruments, ITC 502S). CPL spectra were recorded on a JASCO CPL-300 spectro-fluoropolarimeter for Eu(III) complexes (0.5 mg) mixed with KBr (150 mg). Tablets (diameter: 10 mm, Eu(III) complexes / KBr) were prepared using a PT-10 tablet forming machine (48.2 kN, press time: 3 min).

Computational Details: All quantum chemical calculations were performed by the density functional theory (DFT) with the long-range and dispersion corrected ωB97X-D functional[34] using the Gaussian 16 package.[35] The spin-unrestricted self-consistent field calculations were performed. Excited states were investigated using time-dependent (TD)-DFT. The Stuttgart RSC 1997 (ECP28MWB)[36,37] basis set was adopted for Eu atoms, while the cc-pVDZ basis set[38] was used for the other atoms.

Results and Discussion

Structural characterizations

Chiral Eu(III) coordination polymers with ethynyl linkers, $[Eu(+tfc)_3(m\text{-dpeb})]_n$ and $[Eu(+tfc)_3(p\text{-dpeb})]_n$, were synthesized by complexation of *m*-dpeb and *p*-dpeb with $[Eu(+tfc)_3(H_2O)_2]$ in a methanol solution, respectively. The formation of the coordination polymers was characterized using FT-IR and ESI-MS spectroscopy. The FT-IR spectra of *m*-dpeb, $[Eu(+tfc)_3(H_2O)_2]$, and $[Eu(+tfc)_3(m\text{-dpeb})]_n$ are shown in Figure S5a (SI). The precursor $[Eu(+tfc)_3(H_2O)_2]$ shows significant O-H stretching vibrational signals for coordinated water at approximately 3,400 cm^{-1}. The disappearance of O-H stretching vibrational signals was observed in the IR spectrum of $[Eu(+tfc)_3(m\text{-dpeb})]_n$. The disappearance of coordinated water in *p*-linked $[Eu(+tfc)_3(p\text{-dpeb})]_n$ was also confirmed (SI: Figure S5b).

The ESI-MS spectra and simulated mass patterns of $[Eu(+tfc)_3(m\text{-dpeb})]_n$ are shown in Figure 2. The observed signals with mass numbers (*m*/*z*) of 1173.2, 2592.5, 4013.8, and 5434.1 were assigned to the fragments of $[Eu(+tfc)_2(m\text{-dpeb})]^+$, $[Eu_2(+tfc)_5(m\text{-dpeb})_2]^+$, $[Eu_3(+tfc)_8(m\text{-dpeb})_3]^+$, and $[Eu_4(+tfc)_{11}(m\text{-dpeb})_4]^+$, respectively. Assignments were made by comparing the observed isotope distribution of $[Eu_n(+tfc)_{3n-1}(m\text{-dpeb})_n]^+$ (*m*/*z* at approximately 1173.2, 2592.5, 4013.8, and 5434.1) with the calculated data. The observed ESI-MS signals of *p*-linked $[Eu(+tfc)_3(p\text{-dpeb})]_n$ were also assigned to fragments of $[Eu_n(+tfc)_{3n-1}(p\text{-dpeb})_n]^+$ (SI: Figure S6).

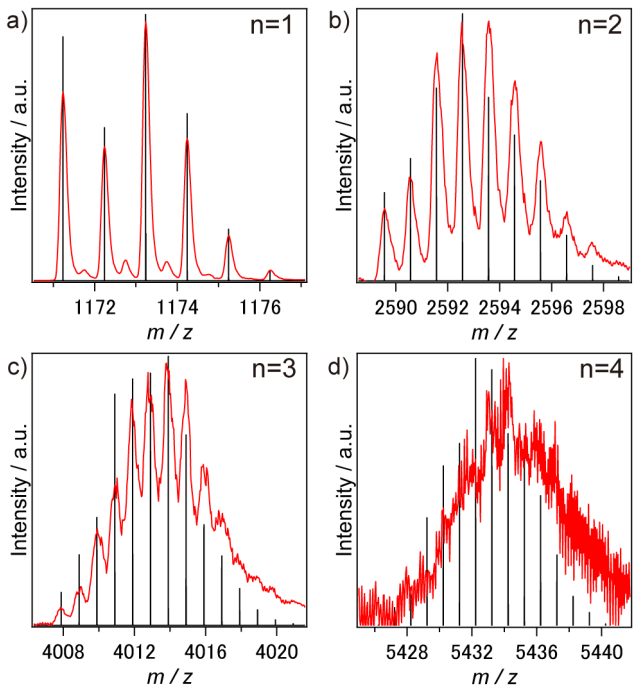

Figure 2. ESI-MS spectra (red) and simulated mass pattern (black) of $[Eu_n(+tfc)_{3n-1}(m\text{-dpeb})_n]^+$: (a) n = 1, b) n = 2, c) n = 3, and d) n = 4).

TG measurements were conducted in a nitrogen atmosphere to evaluate the thermophysical properties of $[Eu(+tfc)_3(m\text{-dpeb})]_n$, $[Eu(+tfc)_3(p\text{-dpeb})]_n$, and the precursor $[Eu(+tfc)_3(H_2O)_2]$. Although the elimination of coordinated water in the precursor $[Eu(+tfc)_3(H_2O)_2]$ was observed at approximately 90 °C , the decomposition temperatures (T_d) of $[Eu(+tfc)_3(m\text{-dpeb})]_n$ and $[Eu(+tfc)_3(p\text{-dpeb})]_n$ were 306 and 298 °C, respectively (Figure 3a). The high decomposition temperatures of $[Eu(+tfc)_3(m\text{-dpeb})]_n$ and $[Eu(+tfc)_3(p\text{-dpeb})]_n$ are similar to those of previously reported chiral lanthanide coordination polymers (T_d > 300 °C).[16,20]

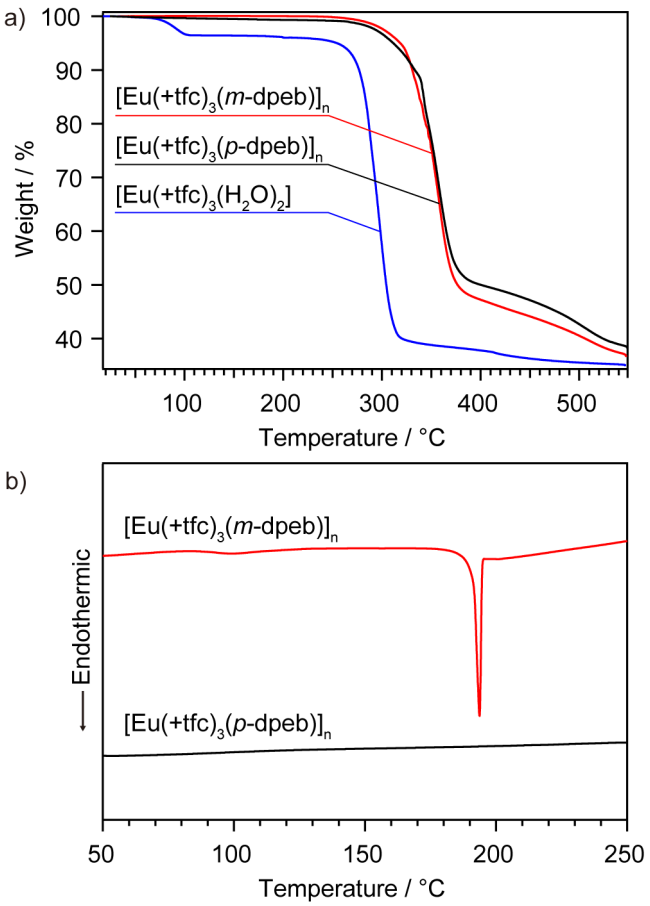

Figure 3. a) TG and b) DSC thermograms of $[Eu(+tfc)_3(m\text{-dpeb})]_n$ (red line), $[Eu(+tfc)_3(p\text{-dpeb})]_n$ (black line), and $[Eu(+tfc)_3(H_2O)_2]$ (blue line) in a nitrogen atmosphere at a heating and cooling rate of 5 °C min^{-1}.

PXRD patterns of $[Eu(+tfc)_3(m\text{-dpeb})]_n$ at various temperatures are shown in Figure 4a. The characteristic peaks at 2θ = 7.5°, 8.0°, 8.4°, 11.0°, 12.9°, 14.3°, 15.0°, 15.3°, 19.3°, 20.2°, and 20.8° were observed under 160 °C (Type-A). We also observed drastic changes in the PXRD patterns of $[Eu(+tfc)_3(m\text{-dpeb})]_n$ at 2θ = 7.9°, 9.1°, 15.1°, 19.9°, and 20.4° at 180 °C, which were related to the phase-transition behavior. The peaks disappeared due to the melting of the Eu(III) coordination polymer at 200 °C .

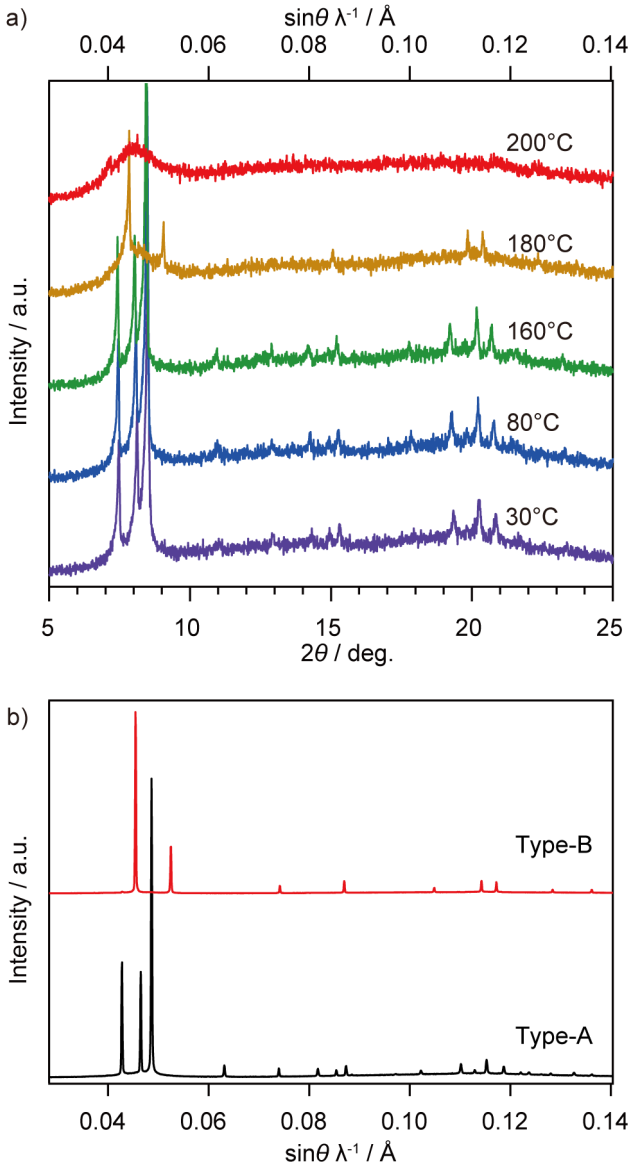

Figure 4. a) PXRD patterns of $[Eu(+tfc)_3(m\text{-dpeb})]_n$ in the temperature range of 30–200 °C. b) Synchrotron PXRD patterns of $[Eu(+tfc)_3(m\text{-dpeb})]_n$ measured at 23 °C after the heat-treatment (black line: Type-A; red line: Type-B).

Based on the DSC measurements, characteristic endothermic peaks corresponding to the phase-transition and melting phenomena of $[Eu(+tfc)_3(m\text{-dpeb})]_n$ were observed at 192 °C (Figure 3b). In the DSC thermogram expanded the region at 130–200 °C, the transformation behavior is making slow progress (SI: Figure S8). A significant endothermic peak of $[Eu(+tfc)_3(p\text{-dpeb})]_n$ was not visible. These results indicate that $[Eu(+tfc)_3(m\text{-dpeb})]_n$ exhibits three stable structures (Type-A, Type-B, and melting states) depending on the temperature.

To confirm the stable structure of the coordination polymer at room temperature, synchrotron PXRD measurements of $[Eu(+tfc)_3(m\text{-dpeb})]_n$ were performed after heat-treatment (Figure 4b). The PXRD patterns of phase-transformed $[Eu(+tfc)_3(m\text{-dpeb})]_n$ after heat-treatment at 180 °C for 30 min and rapid cooling (Type-B) agreed with those obtained under heating (Figure 4a; at 180 °C). The Type-B structure of $[Eu(+tfc)_3(m\text{-dpeb})]_n$ was maintained in air at room temperature. The additional PXRD measurements were conducted to check the stable structure of $[Eu(+tfc)_3(m\text{-dpeb})]_n$ after heating at 200 °C (melting state) and cooling. The PXRD patterns of the coordination polymer after heat-treatment at 200 °C and rapid (c.a. 100 °C min^{-1}, Type-C) or slow (c.a. 1 °C min^{-1}, Type-D) cooling are shown in Figure S9 (SI). The PXRD patterns of Type-C (rapid cooling from 200 °C) agreed with those of Type-B (rapid cooling from 180 °C). On the other hands, the PXRD patterns of Type-D (slow cooling from 200 °C) showed presence of phase A and B. This result indicates that the structural phase of Type-B was metastable and partially transformed back into phase A.

The PXRD patterns of *p*-linked $[Eu(+tfc)_3(p\text{-dpeb})]_n$ were not transformed in the heat-treatment below the decomposition temperature (SI: Figure S10). We successfully prepared the orientation-change Type-A and Type-B samples of $[Eu(+tfc)_3(m\text{-dpeb})]_n$ based on the phase-transition.

Photophysical properties

The excitation and emission spectra of Type-A at room temperature are shown in Figure 5a. The sharp excitation bands at 464, 525, and 534 nm are attributed to the 4f-4f transitions of Eu(III) ($^5D_2 \leftarrow {}^7F_0$, $^5D_1 \leftarrow {}^7F_0$, and $^5D_1 \leftarrow {}^7F_1$).[39] The broad excitation bands are attributed to the π-π* transitions in the organic ligands. The emission bands at 578, 590, 612, 652, and 700 nm are attributed to the 4f-4f transitions of Eu(III) ($^5D_0 \rightarrow {}^7F_J$: J = 0, 1, 2, 3, and 4).[39] The emission spectra of Type-A and Type-B expanded in the region of $^5D_0 \rightarrow {}^7F_{0,1}$ and $^5D_0 \rightarrow {}^7F_2$ transitions are shown in Figure 5b and 5c, respectively. The spectral shape with Stark splitting at the magnetic dipole transition ($^5D_0 \rightarrow {}^7F_1$) and electric dipole transition ($^5D_0 \rightarrow {}^7F_2$) of Type-A agreed with that of Type-B. The agreement between the transition bands reveals that the geometrical structure around the Eu(III) center in Type-A is the same as that in Type-B.

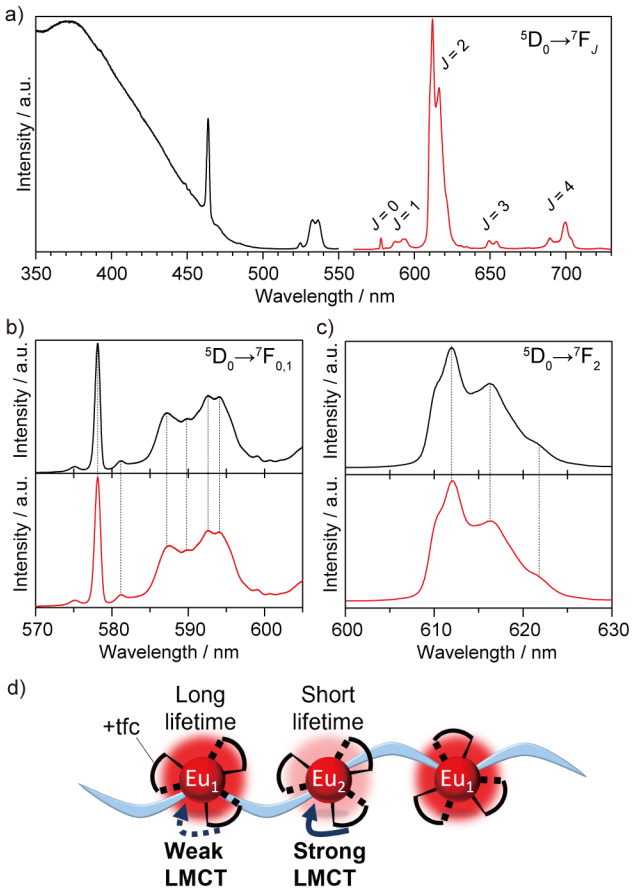

Figure 5. a) Excitation (black, λ_{em} = 612 nm) and emission spectra (red, λ_{ex} = 360 nm) of Type-A measured at room temperature; b), c) Emission spectra (λ_{em} = 612 nm) of Type-A (black) and Type-B (red) expanded the region of $^5D_0 \rightarrow {}^7F_{0,1}$ and $^5D_0 \rightarrow {}^7F_2$ transitions, respectively. d) Schematic image of two emission sites of Eu(III) coordination polymer.

The time-resolved emission decay profiles obtained for Type-A and -B at room temperature are shown in Figure S11 (SI). Double-exponential decays with sub-millisecond scale lifetimes were observed. The multi-exponential decay might arise from the two emission sites of the Eu(III) ion (Figure 5d), which is a common behavior in inorganic phosphors including lanthanide ions.[40] The emission lifetimes and their ratios were estimated using an exponential

function (Table 1). The shorter lifetime (τ_2) may be due to non-radiative relaxation via the LMCT quenching process. That LMCT quenching process often occurs in chiral Eu(III) complexes with camphor ligands.[12,41] The average emission lifetime (τ_{ave}) of Type-B (270 μs) was slightly longer than that of Type-A (253 μs). Based on the emission lifetime and emission spectra, the 4f-4f emission quantum yield ($\Phi_{f\text{-}f}$), radiative rate constant (k_r), and non-radiative rate constant (k_{nr}) were estimated using the following equations:

$$k_r = \frac{1}{\tau_{rad}} = A_{MD,0} n^3 \frac{I_{tot}}{I_{MD}}, \qquad (2)$$

$$\Phi_{f\text{-}f} = \frac{k_r}{k_r + k_{nr}} = \frac{\tau_{obs}}{\tau_{rad}}, \qquad (3)$$

$$k_{nr} = \frac{1}{\tau_{obs}} - \frac{1}{\tau_{rad}}, \qquad (4)$$

where τ_{obs} and τ_{rad} are the observed and radiative emission lifetimes, respectively. τ_{rad} is defined as the ideal emission lifetime without a non-radiative process. In these calculations, we used the τ_{ave} value as the τ_{obs} unit. The parameter $A_{MD,0}$, n, and the calculated I_{tot}/I_{MD} are the spontaneous emission probability for the $^5D_0 \rightarrow {}^7F_1$ transition *in vacuo* (14.65 s^{-1}), the refractive index of the medium (n = 1.5), and the ratio of the total area of the corrected Eu(III) emission spectrum to the area of the $^5D_0 \rightarrow {}^7F_1$ band, respectively.[42] These photophysical parameters of Type-A and Type-B are summarized in Table 1.

Table 1. Photophysical properties of $[Eu(+tfc)_3(m\text{-dpeb})]_n$.

	τ_1 / μs	τ_2 / μs	τ_{ave} / μs	k_r / s^{-1}	k_{nr} / s^{-1}	$\Phi_{f\text{-}f}$ / %	g_{CPL} (at 594 nm)	g_{CPL} (at 613 nm)
Type-A	322 (69%)	98 (31%)	253	1.07×10^3	2.88×10^3	27	−0.092	+0.008
Type-B	340 (70%)	109 (30%)	270	1.06×10^3	2.64×10^3	29	−0.030	+0.002

The k_r value of Type-A (1.07×10^3 s^{-1}) was almost the same as that of Type-B (1.06×10^3 s^{-1}). On the other hand, the k_{nr} value of Type-A (2.88×10^3 s^{-1}) was larger than that of Type-B (2.64×10^3 s^{-1}). From the temperature-dependent emission lifetime measurements and kinetic analyses (SI: Figures S12, S13, and S14 and Table S1), the activation energy (ΔE_a) and frequency factor (A) of the back energy transfer from Eu(III) to LMCT states were estimated. The calculated ΔE_a value of Type-A (2,200 cm^{-1}) was larger than that of Type-B (1,880 cm^{-1}). The calculated A value of Type-A (1.1×10^8 s^{-1}) was almost five times larger than that of Type-B (2.0×10^7 s^{-1}). The LMCT states of $[Eu(+tfc)_3(m\text{-dpeb})]_n$ is influenced by the change in molecular orientation based on the phase-transition.

The CPL spectra of the two types of $[Eu(+tfc)_3(m\text{-dpeb})]_n$ (Type-A and Type-B) in the solid state (in KBr pellets) are shown in Figure 6. Characteristic CPL signals were observed at approximately 580–600 ($^5D_0\rightarrow{}^7F_1$) and 610–620 nm ($^5D_0\rightarrow{}^7F_2$). In the magnetic dipole transition ($^5D_0\rightarrow{}^7F_1$), two significant peaks were observed at 586 and 594 nm for each coordination polymer. The intensity of the negative CPL signal in Type-A was larger than that in Type-B in this region. The maximum $|g_{CPL}|$ value for Type-A (g_{CPL} = −0.092) was three times larger than that for Type-B (g_{CPL} = −0.030). In the electric dipole transition ($^5D_0\rightarrow{}^7F_2$), the $|g_{CPL}|$

value of Type-A was also larger than that of Type-B. The significantly large difference in the $|g_{CPL}|$ values between Type-A and Type-B might be affected by the molecular orientation of the polymer chains.

To confirm the effect of molecular orientation on the CPL properties in Eu(III) coordination polymer, we demonstrated amorphization via an additive phosphine oxide ligand (SI: Figures S15 and S16). After amorphization, amorphized Type-A exhibited a decreasing $|g_{CPL}|$ value (g_{CPL} = −0.076), which agrees with that for amorphized Type-B (g_{CPL} = −0.077). These additional experiments indicated that the g_{CPL} value depends on the orientation of the polymer chains in the solid state.

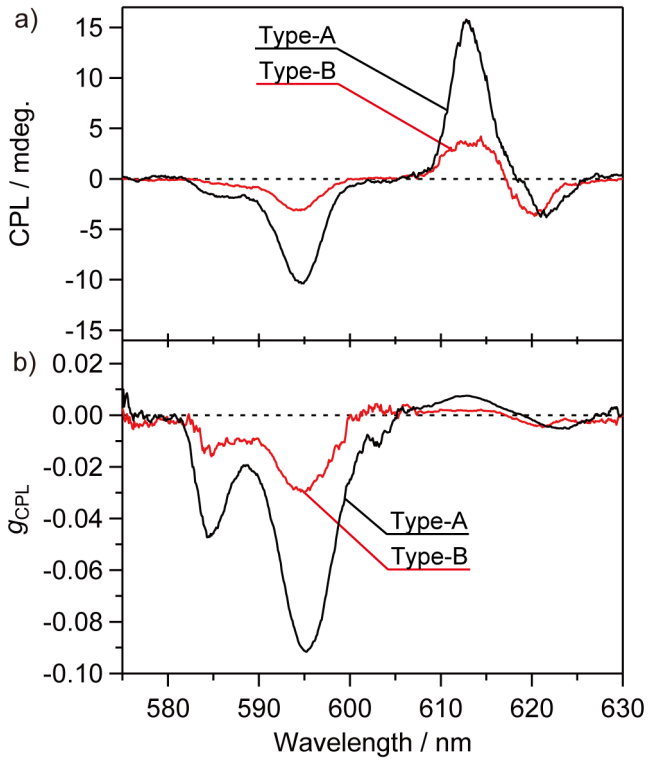

Figure 6. a) CPL and b) g_{CPL} spectra (λ_{ex} = 350 nm) of $[Eu(+tfc)_3(m\text{-dpeb})]_n$ measured at room temperature after heat-treatment (in KBr pellet; black line: Type-A; red line: Type-B)

DFT calculations

Recently, the photophysical and theoretical analyses of the LMCT excited states, which affect the 4f-4f transition probability in Eu(III) complexes, have been focused.[43–45] We considered that the chiroptical properties of chiral Eu(III) compounds are also affected by the LMCT transition. Thus, the transition electric dipole moments of the LMCT states were estimated by TD-DFT calculations to understand the mechanism of the g_{CPL} change under structural transformation. The TD-DFT calculations were performed using a mononuclear chiral Eu(III) complex with camphor ligands, [Eu(+tfc)$_3$(tppo)$_2$] (tppo: triphenylphosphine oxide), as a one-unit model.[18] A dimer model (Eu-Eu distance: $d_{Eu\text{-}Eu}$ = 12.79 Å) was constructed from the X-ray crystallographic data. The modified structures elongating the Eu-Eu distance of the original dimer model to $d_{Eu\text{-}Eu}$ = 13, 14, and 15 Å (Figure 7a) were also examined by the TD-DFT calculations.

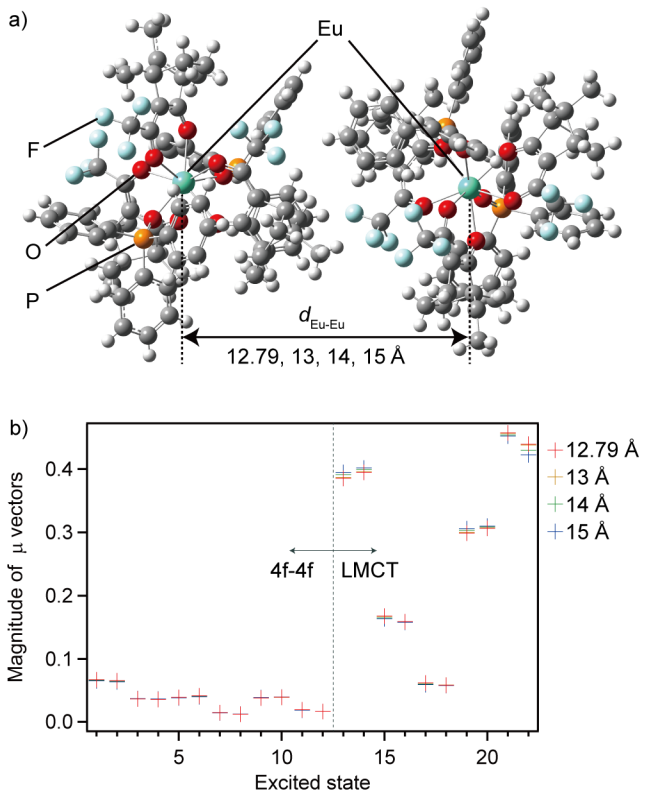

Figure 7. a) Molecular structure of Eu(+tfc)$_3$(tppo)$_2$ dimer model. b) Magnitude of transition electric dipole moment vectors ($|\vec{\mu}|$) in 4f-4f or LMCT excited states.

The calculated excitation energies and transition assignments are summarized in Tables 2, S2, S3, and S4 (SI). The 4f-4f transition character was observed for the excited states 1 through 12 in Table 2. LMCT nature was observed for the excited states 13 to 22. Based on the calculation data, the magnitudes of the transition electric dipole moments ($|\vec{\mu}|$) in the excited states 1–22 are shown in Figure 7b. The $|\vec{\mu}|$ in the LMCT transitions was slightly dependent on the Eu-Eu distance, although the $|\vec{\mu}|$ in the region of 4f-4f transitions was almost unchanged. Furthermore, the $|\vec{\mu}|$ in the LMCT transitions was also dependent on the direction between the units (SI: Figure S18).

Table 2. Excitation energies of Eu(+tfc)$_3$(tppo)$_2$ dimer model ($d_{Eu\text{-}Eu}$ = 12.79 Å) obtained by TD-DFT calculation.

excited state	excitation energy / cm^{-1}	oscillator strength	largest configuration	character	splitting energy gap (ΔE_{split}) / cm^{-1}
1	1,047	0.0000	HOMO−128 → LUMO+1 (α)	4f-4f	7
2	1,054	0.0000	HOMO−132 →LUMO (α)	4f-4f	
3	1,776	0.0000	HOMO−148 → LUMO+1 (α)	4f-4f	2
4	1,778	0.0000	HOMO−157 →LUMO (α)	4f-4f	
5	1,972	0.0000	HOMO−148 → LUMO+1 (α)	4f-4f	4
6	1,976	0.0000	HOMO−149 →LUMO (α)	4f-4f	
7	2,429	0.0000	HOMO−114 → LUMO+1 (α)	4f-4f	7
8	2,436	0.0000	HOMO−120 →LUMO (α)	4f-4f	
9	3,431	0.0000	HOMO−100 →LUMO (α)	4f-4f	6
10	3,437	0.0000	HOMO−95 → LUMO+1 (α)	4f-4f	
11	3,671	0.0000	HOMO−117 →LUMO (α)	4f-4f	2
12	3,673	0.0000	HOMO−110 → LUMO+1 (α)	4f-4f	
13	12,110	0.0055	HOMO−1 →LUMO (α)	LMCT	203
14	12,313	0.0058	HOMO → LUMO+1 (α)	LMCT	
15	15,675	0.0013	HOMO−3 →LUMO (α)	LMCT	198
16	15,873	0.0012	HOMO−2→ LUMO+1 (α)	LMCT	
17	16,393	0.0002	HOMO−4→ LUMO+1 (α)	LMCT	577
18	16,970	0.0002	HOMO−5 →LUMO (α)	LMCT	
19	20,169	0.0055	HOMO−8 →LUMO (α)	LMCT	191
20	20,360	0.0058	HOMO−7→ LUMO+1 (α)	LMCT	
21	20,584	0.0131	HOMO−6→ LUMO+1 (α)	LMCT	101
22	20,685	0.0121	HOMO−9 →LUMO (α)	LMCT	

Theoretically, the energy levels of the LMCT transition in the dimer model are split into LMCT states 1 and 2 because of the interactions between the two Eu(III) units (Figure 8a). To estimate the quantum mixing between the LMCT and 4f-4f states, we considered the contribution of the splitting energy gap (ΔE_{split}). The relationship between ΔE_{split} and $d_{Eu\text{-}Eu}$ is shown in Figure 8b. The large ΔE_{split} in short $d_{Eu\text{-}Eu}$ leads to a small energy gap between the LMCT and 4f-4f states ($\Delta E_{LMCT\text{-}4f}$ in Figure 8a), resulting in a large quantum mixing of the LMCT and 4f-4f states. The images of the molecular orbitals with the largest ΔE_{split} (excited states 17 and 18) are shown in Figure 8c, where the characteristic LMCT transitions (π (+tfc)→4f (Eu)) were observed. These results suggest that the molecular orientation of chiral Eu(III) compounds affects the splitting energy of LMCT states (ΔE_{split}) and their quantum mixing ($\Delta E_{LMCT\text{-}4f}$), resulting in a change in g_{CPL} because of structural transformation.

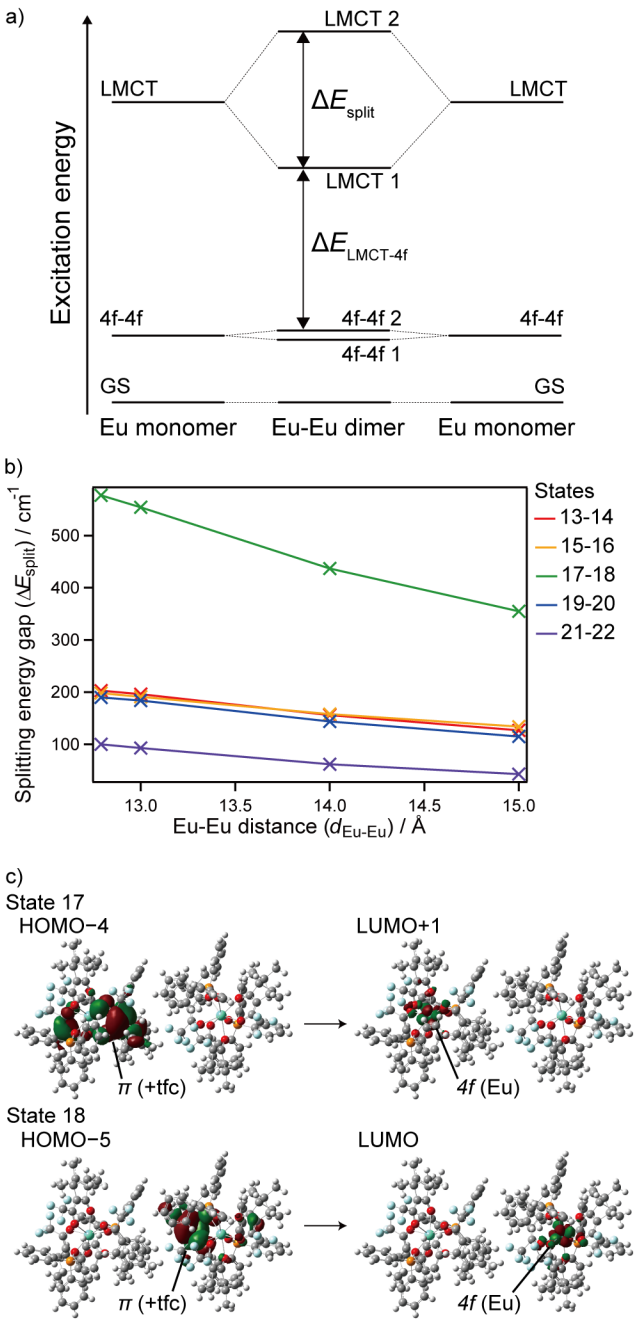

Figure 8. a) Energy diagrams of correlations between 4f-4f and LMCT states for monomer and dimer model. b) Relationship between splitting energy gap (ΔE_{split}) and Eu-Eu distance (d_{Eu-Eu}). c) Selected α-spin molecular orbitals of $Eu(+tfc)_3(tppo)_2$ dimer model (d_{Eu-Eu} = 12.79Å).

Conclusions

Novel chiral Eu(III) coordination polymers, $[Eu(+tfc)_3(p\text{-dpeb})]_n$ and $[Eu(+tfc)_3(m\text{-dpeb})]_n$, were synthesized. $[Eu(+tfc)_3(m\text{-dpeb})]_n$ showed phase-transition behavior at 180 °C, whereas $[Eu(+tfc)_3(p\text{-dpeb})]_n$ showed no phase-transition behavior. The phase-transition behavior of Eu(III) coordination polymers was depended on the position of the ethynyl groups in the phosphine oxide ligands. The emission spectra (coordination geometrical analyses) and CPL measurements (chiroptical properties) showed that the dissymmetry factor (g_{CPL}) is related to the orientation of the polymer chains in the crystalline solid. The photophysical findings were confirmed by performing quantum chemical calculations.

Further control of the orientation of the polymer chains in chiral Eu(III) coordination polymers can improve the $|g_{CPL}|$ value for optical applications such as security tags and three-dimensional displays. The relationship between the molecular orientation and the CPL properties of chiral Eu(III) compounds opens up a frontier fields of coordination chemistry, material science, and solid-state photophysical chemistry.

ASSOCIATED CONTENT

The Supporting Information is available free of charge.

Schematic reaction of Eu(III) coordination polymers and complex including ethynyl group in the linker ligand; ^{1}H and ^{31}P NMR spectra; FT-IR spectra; ESI-MS spectra; DSC thermograms and PXRD patterns of $[Eu(+tfc)_3(m\text{-dpeb})]_n$; PXRD patterns of $[Eu(+tfc)_3(p\text{-dpeb})]_n$; Emission decay profiles of $[Eu(+tfc)_3(m\text{-dpeb})]_n$; Temperature-dependent emission lifetimes and Arrhenius plots of $[Eu(+tfc)_3(m\text{-dpeb})]_n$; PXRD patterns, emission spectra, and g_{CPL} spectra of $[Eu(+tfc)_3(m\text{-dpeb})]_n$ after amorphization (PDF)

AUTHOR INFORMATION

Corresponding Author

Yasuchika Hasegawa − Faculty of Engineering, Hokkaido University, Kita 13, Nishi 8, Kita-ku Sapporo, Hokkaido 060-8628, Japan; Institute for Chemical Reaction Design and Discovery (WPI-ICReDD), Hokkaido University, Kita 21, Nishi 10, Kita-ku, Sapporo, Hokkaido 001-0021, Japan.

Tel. /Fax: +81-11-706-7114.

E-mail: hasegaway@eng.hokudai.ac.jp

Authors

Makoto Tsurui – Graduate School of Chemical Sciences and Engineering, Hokkaido University, Kita 13, Nishi 8, Kita-ku, Sapporo, Hokkaido 060-8628, Japan.

Yuichi Kitagawa – Faculty of Engineering, Hokkaido University, Kita 13, Nishi 8, Kita-ku Sapporo, Hokkaido 060-8628, Japan; Institute for Chemical Reaction Design and Discovery (WPI-ICReDD), Hokkaido University, Kita 21, Nishi 10, Kita-ku, Sapporo, Hokkaido 001-0021, Japan.

Sunao Shoji – Faculty of Engineering, Hokkaido University, Kita 13, Nishi 8, Kita-ku Sapporo, Hokkaido 060-8628, Japan; Institute for Chemical Reaction Design and Discovery (WPI-ICReDD), Hokkaido University, Kita 21, Nishi 10, Kita-ku, Sapporo, Hokkaido 001-0021, Japan.

Hitomi Ohmagari – College of Science and Engineering, Aoyama Gakuin University, 5-10-1 Fuchinobe, Chuo-ku, Sagamihara, Kanagawa 252-5258, Japan.

Miki Hasegawa – College of Science and Engineering, Aoyama Gakuin University, 5-10-1 Fuchinobe, Chuo-ku, Sagamihara, Kanagawa 252-5258, Japan.

Masayuki Gon – Graduate School of Engineering, Kyoto University, Kyoto daigaku-katsura, Nishikyo-ku, Kyoto 615-8510, Japan.

Kazuo Tanaka – Graduate School of Engineering, Kyoto University, Kyoto daigaku-katsura, Nishikyo-ku, Kyoto 615-8510, Japan.

Masato Kobayashi – Faculty of Science, Hokkaido University, Kita 10, Nishi 8, Kita-ku, Sapporo, Hokkaido 060-0810, Japan; Institute for Chemical Reaction Design and Discovery (WPI-ICReDD), Hokkaido University, Kita 21, Nishi 10, Kita-ku, Sapporo, Hokkaido 001-0021, Japan.

Tetsuya Taketsugu – Faculty of Science, Hokkaido University, Kita 10, Nishi 8, Kita-ku, Sapporo, Hokkaido 060-0810, Japan; Institute for Chemical Reaction Design and Discovery

(WPI-ICReDD), Hokkaido University, Kita 21, Nishi 10, Kita-ku, Sapporo, Hokkaido 001-0021, Japan.

Koji Fushimi – Faculty of Engineering, Hokkaido University, Kita 13, Nishi 8, Kita-ku Sapporo, Hokkaido 060-8628, Japan.

Notes

The authors declare no competing financial interest.

ACKNOWLEDGMENT

This work was supported by JSPS KAKENHI Grants Number JP20H02748, JP20H04653, JP20H05197, JP20K21201, JP21K18969, JP22K14741, JP17H06374, and JP20K15041 of the Ministry of Education, Culture, Sports, Science, and Technology (MEXT) of Japan. This work was also supported by the Institute for Chemical Reaction Design and Discovery (ICReDD), established by the World Premier International Research Initiative (WPI) and JSPS Research Fellowship for Young Scientist (JP21J20980) of MEXT, Japan. The synchrotron radiation experiments were performed at the BL02B2 of SPring-8 with the approval of the Japan Synchrotron Radiation Research Institute (Proposal No. 2020A1451 and 2021B1262). The authors express sincere thanks to Prof. Hajime Ito of Hokkaido University and Dr. Tomohiro Seki of Shizuoka University for measurements of temperature-dependent X-ray diffraction.

ABBREVIATIONS

Eu, europium; CPL, circularly polarized luminescence; LMCT, ligand-to-metal charge transfer; DFT, density functional theory; TG, thermogravimetry; DSC differential scanning calorimetry; PXRD, powder X-ray diffraction

REFERENCES

(1) Richardson, F. S.; Riehl, J. P.; Richardson, F. S.; Riehl, J. P. Circularly Polarized Luminescence Spectroscopy. *Chem. Rev.* **1977**, *77*, 773–792.

(2) Mason, S. F. *Molecular Optical Activity and the Chiral Discriminations*; Cambridge University Press, 1982.

(3) Berova, N.; Nakanishi, K.; W. Woody, R. *Circular Dichroism : Principles and Applications*, 2nd ed.; 2000.

(4) Kitagawa, Y.; Wada, S.; Islam, M. D. J.; Saita, K.; Tanaka, K.; Maeda, S.; Hasegawa, Y. Chiral Lanthanide Lumino-Glass for a Circularly Polarized Light Security Device. *Commun. Chem.* **2020**, *3*, 119–123.

(5) Sang, Y.; Han, J.; Zhao, T.; Duan, P.; Liu, M. Circularly Polarized Luminescence in Nanoassemblies: Generation, Amplification, and Application. *Adv. Mater.* **2020**, *32*, 1900110.

(6) Zinna, F.; Pasini, M.; Galeotti, F.; Botta, C.; Di Bari, L.; Giovanella, U. Design of Lanthanide-Based OLEDs with Remarkable Circularly Polarized Electroluminescence. *Adv. Funct. Mater.* **2017**, *27*, 1603719.

(7) Song, F.; Xu, Z.; Zhang, Q.; Zhao, Z.; Zhang, H.; Zhao, W.; Qiu, Z.; Qi, C.; Zhang, H.; Sung, H. H. Y. et al., Highly Efficient Circularly Polarized Electroluminescence from Aggregation-Induced Emission Luminogens with Amplified Chirality and Delayed Fluorescence. *Adv. Funct. Mater.* **2018**, *28*, 1–12.

(8) Lunkley, J. L.; Nguyen, N. M.; Tuminaro, K. M.; Margittai, D.; Muller, G. The Importance of Solvent Effects on the Mechanism of the Pfeiffer Effect. *Inorganics* **2018**, *6*, 87–112.

(9) Muller, G. Luminescent Chiral Lanthanide(III) Complexes as Potential Molecular Probes. *Dalton Trans.* **2009**, 9692–9707.

(10) Carr, R.; Evans, N. H.; Parker, D. Lanthanide Complexes as Chiral Probes Exploiting Circularly Polarized Luminescence. *Chem. Soc. Rev.* **2012**, *41*, 7673–7686.

(11) Zinna, F.; Di Bari, L. Lanthanide Circularly Polarized Luminescence: Bases and Applications. *Chirality* **2015**, *27*, 1–13.

(12) Kitagawa, Y.; Tsurui, M.; Hasegawa, Y. Steric and Electronic Control of Chiral Eu(III) Complexes for Effective Circularly Polarized Luminescence. *ACS Omega* **2020**, *5*, 3786–3791.

(13) Brittain, H. G.; Richardson, F. S. Circularly Polarized Emission Studies on the Chiral Nuclear Magnetic Resonance Lanthanide Shift Reagent Tris(3-Trifluoroacetyl-d-Camphorato)Europium(III). *J. Am. Chem. Soc.* **1976**, *98*, 5858–5863.

(14) Gong, J.; Zhang, X. Coordination-Based Circularly Polarized Luminescence Emitters: Design Strategy and Application in Sensing. *Coord. Chem. Rev.* **2022**, *453*, 214329.

(15) Ma, K.; Chen, W.; Jiao, T.; Jin, X.; Sang, Y.; Yang, D.; Zhou, J.; Liu, M.; Duan, P. Boosting the Circularly Polarized Luminescence of Small Organic Molecules: Via Multi-Dimensional Morphology Control. *Chem. Sci.* **2019**, *10*, 6821–6827.

(16) Hasegawa, Y.; Miura, Y.; Kitagawa, Y.; Wada, S.; Nakanishi, T.; Fushimi, K.; Seki, T.; Ito, H.; Iwasa, T.; Taketsugu, T. et al., K. Spiral Eu(iii) Coordination Polymers with Circularly Polarized Luminescence. *Chem. Commun.* **2018**, *54*, 10695–10697.

(17) Wada, S.; Kitagawa, Y.; Nakanishi, T.; Gon, M.; Tanaka, K.; Fushimi, K.; Chujo, Y.; Hasegawa, Y. Electronic Chirality Inversion of Lanthanide Complex Induced by Achiral Molecules. *Sci. Rep.* **2018**, *8*, 1–9.

(18) Harada, T.; Nakano, Y.; Fujiki, M.; Naito, M.; Kawai, T.; Hasegawa, Y. Circularly Polarized Luminescence of Eu(III) Complexes with Point- and Axis-Chiral Ligands Dependent on Coordination Structures. *Inorg. Chem.* **2009**, *48*, 11242–11250.

(19) Harada, T.; Tsumatori, H.; Nishiyama, K.; Yuasa, J.; Hasegawa, Y.; Kawai, T. Nona-Coordinated Chiral Eu(III) Complexes with Stereoselective Ligand-Ligand Noncovalent Interactions for Enhanced Circularly Polarized Luminescence. *Inorg. Chem.* **2012**, *51*, 6476–6485.

(20) Koiso, N.; Kitagawa, Y.; Nakanishi, T.; Fushimi, K.; Hasegawa, Y. Eu(III) Chiral Coordination Polymer with a Structural Transformation System. *Inorg. Chem.* **2017**, *56*, 5741–5747.

(21) Tan, Y. B.; Okayasu, Y.; Katao, S.; Nishikawa, Y.; Asanoma, F.; Yamada, M.; Yuasa, J.; Kawai, T. Visible Circularly Polarized Luminescence of Octanuclear Circular Eu(III) Helicate. *J. Am. Chem. Soc.* **2020**, *142*, 17653–17661.

(22) Arrico, L.; Benetti, C.; Di Bari, L. Combining Lanthanides with PyBox Ligands: A Simple Route to Circularly Polarized Light Emitters. *ChemPhotoChem* **2021**, *5*, 815–821.

(23) Abhervé, A.; Mastropasqua Talamo, M.; Vanthuyne, N.; Zinna, F.; Di Bari, L.; Grasser, M.; Le Guennic, B.; Avarvari, N. Chiral Emissive Lanthanide Complexes from Enantiopure [6]Helicene-Bis(Pyrazolyl)-Pyridine Ligands. *Eur. J. Inorg. Chem.* **2022**, e202200010.

(24) Zhou, Y.; Yao, Y.; Cheng, Z.; Gao, T.; Li, H.; Yan, P. Point Chirality Controlled Diastereoselective Self-Assembly and Circularly Polarized Luminescence in Quadruple-Stranded Europium(III) Helicates. *Inorg. Chem.* **2020**, *59*, 12850–12857.

(25) Yuasa, J.; Ueno, H.; Kawai, T. Sign Reversal of a Large Circularly Polarized Luminescence Signal by the Twisting Motion of a Bidentate Ligand. *Chem. Eur. J.* **2014**, *20*, 8621–8627.

(26) Tsurui, M.; Kitagawa, Y.; Fushimi, K.; Gon, M.; Tanaka, K.; Hasegawa, Y. Electronic Strain Effect on Eu(III) Complexes for Enhanced Circularly Polarized Luminescence. *Dalton Trans.* **2020**, *49*, 5352–5361.

(27) Kumar, J.; Marydasan, B.; Nakashima, T.; Kawai, T.; Yuasa, J. Chiral Supramolecular Polymerization Leading to Eye Differentiable Circular Polarization in Luminescence. *Chem. Commun.* **2016**, *52*, 9885–9888.

(28) Miyata, K.; Ohba, T.; Kobayashi, A.; Kato, M.; Nakanishi, T.; Fushimi, K.; Hasegawa, Y. Thermostable Organo-Phosphor: Low-Vibrational Coordination Polymers That Exhibit Different Intermolecular Interactions. *ChemPlusChem* **2012**, *77*, 277–280.

(29) Kitagawa, Y.; Kumagai, M.; Ferreira da Rosa, P. P.; Fushimi, K.; Hasegawa, Y. Long-Range LMCT Coupling in Eu III Coordination Polymers for an Effective Molecular Luminescent Thermometer. *Chem. Eur. J.* **2021**, *27*, 264–269.

(30) Zhang, H.; Zhou, L.; Wei, J.; Li, Z.; Lin, P.; Du, S. Highly Luminescent and Thermostable Lanthanide-Carboxylate Framework Materials with Helical Configurations. *J. Mater. Chem.* **2012**, *22*, 21210–21217.

(31) Hirai, Y.; Nakanishi, T.; Kitagawa, Y.; Fushimi, K.; Seki, T.; Ito, H.; Fueno, H.; Tanaka, K.; Satoh, T.; Hasegawa, Y. Luminescent Coordination Glass: Remarkable Morphological Strategy for Assembled Eu(III) Complexes. *Inorg. Chem.* **2015**, *54*, 4364–4370.

(32) Hirai, Y.; Ferreira Da Rosa, P. P.; Nakanishi, T.; Kitagawa, Y.; Fushimi, K.; Hasegawa, Y. Amorphous Formability and Temperature-Sensitive Luminescence of Lanthanide Coordination Glasses Linked by Thienyl, Naphthyl, and Phenyl Bridges with Ethynyl Groups. *Bull. Chem. Soc. Jpn.* **2017**, *90*, 322–326.

(33) Kawaguchi, S.; Takemoto, M.; Osaka, K.; Nishibori, E.; Moriyoshi, C.; Kubota, Y.; Kuroiwa, Y.; Sugimoto, K. High-Throughput Powder Diffraction Measurement System Consisting of Multiple MYTHEN Detectors at Beamline BL02B2 of SPring-8. *Rev. Sci. Instrum.* **2017**, *88*, 085111.

(34) Chai, J. Da; Head-Gordon, M. Long-Range Corrected Hybrid Density Functionals with Damped Atom-Atom Dispersion Corrections. *Phys. Chem. Chem. Phys.* **2008**, *10*, 6615–6620.

(35) Frisch, M. J.; Trucks, G. W.; Schlegel, H. B.; Scuseria, G. E.; Robb, M.; Cheeseman, J. R.; Scalmani, G.; Barone, V.; Petersson, G.; Nakatsuji, H. et al., Gaussian 16; Revision C.01; Gaussian; Inc.; Wallin. 2016.

(36) Dolg, M.; Stoll, H.; Savin, A.; Preuss, H. Energy-Adjusted Pseudopotentials for the Rare Earth Elements. *Theor. Chim. Acta* **1989**, *75*, 173–194.

(37) Pritchard, B. P.; Altarawy, D.; Didier, B.; Gibson, T. D.; Windus, T. L. New Basis Set Exchange: An Open, Up-to-Date Resource for the Molecular Sciences Community. *J. Chem. Inf. Model.* **2019**, *59*, 4814–4820.

(38) Dunning, T. H. Gaussian Basis Sets for Use in Correlated Molecular Calculations. I. The Atoms Boron through Neon and Hydrogen. *J. Chem. Phys.* **1989**, *90*, 1007–1023.

(39) Binnemans, K. Interpretation of Europium (III) Spectra. *Coord. Chem. Rev.* **2015**, *295*, 1–45.

(40) Gupta, S. K.; Reghukumar, C.; Kadam, R. M. Eu^{3+} Local Site Analysis and Emission Characteristics of Novel $Nd_2Zr_2O_7$:Eu Phosphor: Insight into the Effect of Europium Concentration on Its Photoluminescence Properties. *RSC Adv.* **2016**, *6*, 53614–53624.

(41) Lunkley, J. L.; Shirotani, D.; Yamanari, K.; Kaizaki, S.; Muller, G. Extraordinary Circularly Polarized Luminescence Activity Exhibited by Cesium Tetrakis(3-Heptafluoro-

Butylryl-(+)-Camphorato) Eu(III) Complexes in EtOH and $CHCl_3$ Solutions. *J. Am. Chem. Soc.* **2008**, *130*, 13814–13815.

(42) Werts, M. H. V.; Jukes, R. T. F.; Verhoeven, J. W. The Emission Spectrum and the Radiative Lifetime of Eu^{3+} in Luminescent Lanthanide Complexes. *Phys. Chem. Chem. Phys.* **2002**, *4*, 1542–1548.

(43) Kitagawa, Y.; Ferreira Da Rosa, P. P.; Hasegawa, Y. Charge-Transfer Excited States of π- And 4f-Orbitals for Development of Luminescent Eu(iii) Complexes. *Dalton Trans.* **2021**, *50*, 14978–14984.

(44) Islam, M. J.; Kitagawa, Y.; Tsurui, M.; Hasegawa, Y. Strong Circularly Polarized Luminescence of Mixed Lanthanide Coordination Polymers with Control of 4f Electronic Structures. *Dalton Trans.* **2021**, *50*, 5433–5436.

(45) Ferreira Da Rosa, P. P.; Miyazaki, S.; Sakamoto, H.; Kitagawa, Y.; Miyata, K.; Akama, T.; Kobayashi, M.; Fushimi, K.; Onda, K.; Taketsugu, T. et al., Coordination Geometrical Effect on Ligand-to-Metal Charge Transfer-Dependent Energy Transfer Processes of Luminescent Eu(III) Complexes. *J. Phys. Chem. A* **2021**, *125*, 209–217.

TOC Graphic

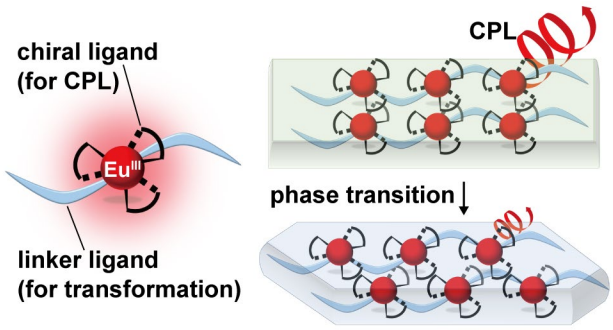
chiral ligand
(for CPL)
Eu^{III}
linker ligand
(for transformation)
CPL
phase transition